

**Molecular simulation of the vapor-liquid equilibria of xylene mixtures
Force field performance, and Wolf vs. Ewald for electrostatic interactions**

Caro-Ortiz, Sebastián; Hens, Remco; Zuidema, Erik; Rigutto, Marcello; Dubbeldam, David; Vlugt, Thijs J.H.

DOI

[10.1016/j.fluid.2018.12.006](https://doi.org/10.1016/j.fluid.2018.12.006)

Publication date

2019

Document Version

Accepted author manuscript

Published in

Fluid Phase Equilibria

Citation (APA)

Caro-Ortiz, S., Hens, R., Zuidema, E., Rigutto, M., Dubbeldam, D., & Vlugt, T. J. H. (2019). Molecular simulation of the vapor-liquid equilibria of xylene mixtures: Force field performance, and Wolf vs. Ewald for electrostatic interactions. *Fluid Phase Equilibria*, 485, 239-247. <https://doi.org/10.1016/j.fluid.2018.12.006>

Important note

To cite this publication, please use the final published version (if applicable).
Please check the document version above.

Copyright

Other than for strictly personal use, it is not permitted to download, forward or distribute the text or part of it, without the consent of the author(s) and/or copyright holder(s), unless the work is under an open content license such as Creative Commons.

Takedown policy

Please contact us and provide details if you believe this document breaches copyrights.
We will remove access to the work immediately and investigate your claim.

Molecular Simulation of the Vapor-Liquid Equilibria of Xylene mixtures: Force Field performance, and Wolf vs. Ewald for Electrostatic Interactions

Sebastián Caro-Ortiz^a, Remco Hens^a, Erik Zuidema^b, Marcello Rigutto^b,
David Dubbeldam^c, Thijs J. H. Vlugt^a

^a*Engineering Thermodynamics, Process & Energy Department, Faculty of Mechanical, Maritime and Materials Engineering, Delft University of Technology, Leeghwaterstraat 39, 2628 CB Delft, The Netherlands*

^b*Shell Global Solutions International, PO Box 38000, 1030 BN, Amsterdam, The Netherlands*

^c*Van 't Hoff Institute of Molecular Sciences, University of Amsterdam, Science Park 904, 1098 XH Amsterdam, The Netherlands*

Abstract

This article explores how well vapor-liquid equilibria of pure components and binary mixtures of xylenes can be predicted using different force fields in molecular simulations. The accuracy of the Wolf method and the Ewald summation is evaluated. Monte Carlo simulations in the Gibbs ensemble are performed at conditions comparable to experimental data, using four different force fields. Similar results using the Wolf and the Ewald methods can be obtained for the prediction of densities and the phase compositions of binary mixtures. With the Wolf method, up to 50% less CPU time is used compared to the Ewald method, at the cost of accuracy and additional parameter calibration. The densities of p-xylene and m-xylene can be well estimated using the TraPPE-UA and AUA force fields. The largest differences of VLE with experiments are observed for o-xylene. The p-xylene/o-xylene binary mixtures at 6.66 and 81.3 kPa are simulated, leading to an excellent agreement in the predictions of the composition of the liquid phase compared to experiments. The composition of the vapor phase is dominated by the properties of the component with the largest mole fraction in the liquid phase. The accuracy of the predictions of the phase composition are related to the quality

Email address: t.j.h.vlugt@tudelft.nl (Thijs J. H. Vlugt)

of the density predictions of the pure component systems. The phase composition of the binary system of xylenes is very sensitive to slight differences in vapor phase density of each xylene isomer, and how well the differences are captured by the force fields.

Keywords: Monte Carlo Simulation, Vapor-Liquid Equilibria, Xylene, Wolf method, Binary mixture

1 Introduction

Xylenes are aromatic species that are mainly produced by the catalytic reforming of crude oil, in a mixture usually containing benzene, toluene and xylenes [1]. Further extraction and distillation processes yield equilibrium mixtures of xylenes that generally contain 53% meta-xylene (mX), 24% ortho-xylene (oX) and 23% para-xylene (pX) [2]. Considering the practical application of each component of the mixture, the separation and further transformation of each isomer is important. From the isomers, pX has the highest economic value [3], and is a core raw material for manufacturing polyester fibers [4]. oX is mostly used in the production of phthalic anhydride [5], while the main component of the mixture, mX, has a limited end use and is preferably isomerized into pX or oX [6]. Xylenes are components of solvents, paint thinners, varnish, corrosion preventives and cleaning agents [7].

Separation of xylenes is a challenge [1, 8, 9, 10]. Separation of oX from the mixture can be achieved by distillation, but this is difficult in the mX/pX case due to similar boiling points [11]. It is considered -with the separation of greenhouse gases from dilute emissions and uranium from seawater- as one of the “*seven chemical separation processes to change the world*” [12]. The separation of xylenes on a large scale is performed by the adsorption in porous materials such as X and Y zeolites [13] or by fractional crystallization [14, 15]. Current research efforts are focused on advances of new membranes and sorbents that decrease the energy consumption of such isomer separation [12]. The accurate description and characterization of the thermodynamic properties, such as the vapor-liquid equilibrium (VLE), is critical for the design of proper techniques, equipment, and processes for an efficient separation [16]. Experimental VLE measurements for xylene mixtures are scarce and only a handful of studies provide data for pure components and binary mixtures of xylenes. For pure component, VLE curves are reported by Smith

30 and Srivastava [17]. For binary mixtures, Rodrigues [18] presented coexis-
31 tence curves for the pX-mX, pX-oX and mX-oX systems at 100.65 kPa. The
32 pX-mX binary system is described by Kato et al. [19] at atmospheric pres-
33 sure. Data for 5, 20, 40 and 101.325 kPa is reported by Onken and Arlt [20].
34 Llopis and Monton [21, 22] reported data for pX-oX and mX-oX systems at
35 6.66 and 26.66 kPa, Parvez et al. [23] characterized the pX-oX coexistence
36 curves at 81.3 kPa. The coexistence of oX-mX at 298.15K is described by
37 Wichterle et al. [24]. Such studies report that binary mixtures of xylenes
38 have small differences from an ideal mixture [18, 19, 20, 21, 23].

39 Molecular simulations are an extensively used tool to predict the thermo-
40 dynamic properties of a wide variety of systems [25]. Fluid phase properties
41 of pure components and mixtures can be computed for large ranges of con-
42 ditions, even when experiments can be challenging, expensive or dangerous
43 [25]. The Monte Carlo (MC) method in the Gibbs ensemble [26] has been
44 widely used to compute VLE [27, 28, 29, 30, 31, 32, 33]. The choice of a
45 force field that accurately describes the interaction potential between atoms
46 and molecules is a crucial factor. The Gibbs ensemble considers two sim-
47 ulation boxes to simulate the properties of coexisting phases avoiding the
48 vapor-liquid interface [27]. Fig. 1 shows the vapor and liquid phases of a
49 xylene mixture in two separate boxes of a *NPT*-Gibbs ensemble MC sim-
50 ulation. Molecular simulations of VLE are typically performed employing
51 force fields that model the interactions with Lennard-Jones potentials (LJ)
52 or a combination of LJ and electrostatic interactions. In the case of aromatic
53 compounds, a common practice in the development of the potentials is to
54 fit the interaction parameters to reproduce the VLE of the pure component
55 [34, 35, 36, 37], or by ab initio quantum mechanical calculations [38, 39, 40].
56 Several force field for xylene interactions have been reported in literature
57 [41, 42, 43, 37, 44, 40], some of which are briefly described in the next sec-
58 tion for further use.

59 The electrostatic interactions are generally represented by charged inter-
60 action sites. The Ewald summation method [45] has been extensively used to
61 account these interactions in periodic systems [46]. The electrostatic energy
62 is calculated in two parts by dividing the potential in a short-range con-
63 tribution computed in real space, and a long-range contribution calculated
64 involving a Fourier transform of the charge density [25]. The long-range
65 contribution constitutes the main disadvantage of the method, it is compu-
66 tationally expensive. Several alternative methods have been developed such
67 as the particle-particle and particle-mesh algorithm [47], the reaction field

68 method [48], the fast multipole algorithm [49], and the Wolf method [50].
69 These methods are reviewed in depth by Cisneros et al. [51]. From these
70 methods, the Wolf method has been effectively applied to a wide variety
71 of systems [52, 53, 54, 55, 56, 57, 58, 59] and has gained attention due to
72 its efficiency compared to the Ewald method as the Fourier part is not of-
73 ten needed in dense systems. To use this method, the cut-off radius (R_c)
74 and the damping factor (α) have to be determined for each system with the
75 procedures described by Hens and Vlucht [60], and Waibel and Gross [61].

76 This article explores how the VLE of pure components and binary mix-
77 tures of xylenes can be predicted using molecular simulations and how well
78 the Wolf method can be applied. The simulation details such as the input
79 and force fields are summarized in Section 2. The simulation results of VLE
80 for pure components and binary mixtures are analyzed in Section 3. The
81 concluding remarks about force field performance and the use of the Wolf
82 method are discussed in Section 4.

83 2. Simulation details

84 The Monte Carlo technique in the Gibbs Ensemble [26] is used for the
85 simulations. The calculations for the VLE of pure components are performed
86 using the Gibbs ensemble at constant total volume (NVT). The isothermal-
87 isobaric version of the Gibbs ensemble (NPT) is used for the binary mixture
88 VLE calculations. The total system contains 1,000 molecules and the inter-
89 actions between different atom types are calculated using Lorentz-Berthelot
90 mixing rules [62]. The LJ interactions are truncated at 14 Å and analytic
91 tail corrections are applied [62]. The Continuous Fractional Component MC
92 (CFCMC) method in the Gibbs ensemble developed by Poursaeidesfahani
93 et al. [63, 64, 65] is used. The Gibbs ensemble is expanded with one ex-
94 tra molecule -the fractional molecule- per molecule type. The fractional
95 molecules have negligible effect on the thermodynamic properties [64]. The
96 interactions of the fractional molecule are scaled in range 0 to 1 (0 for no
97 interactions with surrounding molecules and 1 for full interaction with sur-
98 rounding molecules) described by λ . The trial moves in each MC cycle are
99 selected at random within the following fixed probabilities: 33% translation,
100 33% rotation, 17% changes of the value of λ , 8% identity change of the frac-
101 tional molecule -where the fractional molecule turns into a whole one, while
102 a molecule in the other box turns into a fractional molecule-, 8% swap move
103 -the fractional molecule is transferred from one box to the other-, and 1%

104 volume change. All simulations are performed in an in-house developed code
105 which has been verified to yield the same results as the RASPA software
106 [66, 67]. The number of steps per MC cycle is equal to the total number
107 of molecules in the system. Each simulation starts with 5,000 MC cycles to
108 equilibrate the system by only allowing rotation and translation trial moves.
109 After that, a stage of 40,000 MC cycles initializes the system and all types
110 of trial moves are allowed. In this stage, the Wang-Landau algorithm [68] is
111 used to construct a weight function that flattens the probability distribution
112 of λ , so that all values of λ have the same probability, and that the fractional
113 molecule is equally likely to be found in one of the boxes. The chemical
114 potential is calculated from the probability distribution of λ using the pro-
115 cedure described by Poursaeidesfahani et al. [63]. The initialization stage is
116 followed by a production run of 100,000 MC cycles. The reported errors ac-
117 count for the 95% confidence interval calculated by dividing the production
118 run into five sections.

119 Each simulation starts with a different initial composition (i.e. number of
120 molecules in each box) which is based on the experimental data available for
121 each system. For pure components, the number of molecules and box sizes
122 can be found in the Supporting Information. For binary mixtures, the initial
123 composition can be obtained with the procedure described by Ramdin et al.
124 [27] when experiments are not available. The pX-oX binary mixtures at 6.66
125 kPa and 81.3 kPa are simulated. The initial guess for the side length of the
126 cubic boxes are 60 Å for the liquid phase box and 145 Å for the vapor phase
127 box. Initially, 920 and 80 molecules are assigned to the liquid and vapor
128 boxes, respectively. The guess for the initial phase compositions of each box
129 are chosen to match the experimental phase compositions [21, 23].

130 Four different force fields that model the interactions between xylene iso-
131 mers are used, each one having a particular approach to describe electrostatic
132 interactions. All molecules are defined as rigid and the geometries are ac-
133 cording to the original references [41, 34, 42, 37]. The force field parameters
134 are listed in the Supporting Information. The force fields considered are the
135 following:

136 1. Transferable Potential for Phase Equilibria - United Atom (TraPPE-
137 UA) [41], a widely used force field that is designed to reproduce the VLE
138 of alkylbenzenes as single components. The united atom approach is con-
139 veniently used by merging a carbon atom and its bonded hydrogen atoms
140 into a single uncharged interaction site representing each CH_x group in the
141 aromatic species.

142 2. A modification of the TraPPE-UA force field to include an all-atom
143 approach and charges in the aromatic ring, here called TraPPE-UA-EH. This
144 force field uses the united atom approach from TraPPE-UA [41] to represent
145 the methyl groups, while the bonded carbon and hydrogen atoms from the
146 aromatic ring are individually represented in single interaction centers with
147 charges of $-0.95e$ and $+0.95e$, respectively [34].

148 3. Optimized Potential for Liquid Simulations (OPLS) [42, 69], a widely
149 applied force field that represents the aromatic ring with an all atom ap-
150 proach and the methyl group as a carbon centered atom [70]. Each atom has
151 electrostatic charges.

152 4. Anisotropic United Atom (AUA) [37, 71]. This force field presents
153 a united atom approach, having uncharged single interaction centers for the
154 CH_x groups and positioning the atom in the direction of the center of mass of
155 the atom group, displacing it from the carbon atom position, unlike the other
156 force fields. One of its main features is the representation of the π -cloud in
157 the aromatic ring. One positive partial charge ($+8.13e$) in the center of the
158 ring, and two negative partial charges ($-4.065e$) located at 0.4 \AA above and
159 below the plane of the aromatic ring are introduced. The negative charges
160 are displaced from the center of the ring to reproduce the experimental dipole
161 moment of the molecule.

162 The Ewald summation parameters are chosen such that a relative pre-
163 cision of 10^{-6} is achieved [25]. The Wolf summation parameters are chosen
164 according to the procedure described by Hens and Vlugt [60]. By taking into
165 account the experimental data as a starting point, a short simulation in the
166 NVT ensemble is performed. The chosen density is close to the equilibrium
167 coexistence density. The chosen temperature is above the critical tempera-
168 ture. The system sizes are equal to the initial guess of the box sizes for the
169 binary mixture calculations in the the Gibbs ensemble. From this configura-
170 tion, the electrostatic energy is calculated for several cut-off radii (R_c) and
171 damping factors (α). This energy can be compared to a reference calculated
172 with the Ewald method for the same system configuration. Following this
173 procedure, it is determined that an optimum parameter set for the vapor
174 phase is: $R_c=85 \text{ \AA}$, $\alpha=0.04 \text{ \AA}^{-1}$; and for the liquid phase: $R_c=16 \text{ \AA}$, $\alpha=0.17$
175 \AA^{-1} .

176 3. Results and discussion

177 3.1. Vapor-liquid equilibria of pure components

178 The VLE of pure components are calculated with NVT-Gibbs ensemble
179 Monte Carlo simulations using the CFCMC method [63]. Simulations are
180 performed for each isomer using the Ewald and the Wolf methods. The den-
181 sities for mX are shown in Fig. 2. The calculated coexistence densities for
182 the three isomers with the statistical uncertainties are listed in the Support-
183 ing Information. The differences of the use of the Wolf and Ewald methods
184 for pX and oX computed VLEs are qualitatively the same as for mX. The
185 computed VLEs for the TraPPE-UA-EH and AUA show excellent agreement
186 between the Ewald and Wolf methods. The differences in the calculated den-
187 sities are lower than 1% of the densities and lower than the statistical error
188 of the simulation. The vapor-liquid coexistence densities calculated with the
189 OPLS force field show agreement within the statistical error. The calculated
190 vapor phase densities are underestimated at temperatures between 500 and
191 550 K using the Wolf method. At high temperatures, the size of the vapor
192 phase box and the number of molecules are different than the values used to
193 determine the optimal damping factor α and cut-off radius (R_c). This sug-
194 gests that the vapor density of the system is more sensitive to the choice of
195 the Wolf parameters for the OPLS force field than for the other force fields.
196 The chemical potentials as a function of temperature for the two phases of
197 mX using the Wolf method are shown in Fig. 3. The differences in the chem-
198 ical potential between the phases are within the statistical error. Chemical
199 equilibrium between the vapor and liquid phases is observed as the same
200 chemical potential is calculated for both phases.

201 The vapor-liquid coexistence curves of mX, oX, and pX calculated using
202 the Ewald method are shown in Fig. 4 for each force field. Clear differences
203 can be observed in Fig. 4 for the density calculations with the experimental
204 data. For mX, the TraPPE-UA and the AUA force field predict liquid den-
205 sities that deviate up to 3% from the experimental data, while TraPPE-UA-EH
206 and OPLS force fields show significantly higher differences. The experimen-
207 tal liquid densities of pX are well predicted by TraPPE-UA, TraPPE-UA-EH
208 and AUA, as the difference with the computed density is below the statistical
209 error. The OPLS force field shows slightly higher differences of up to 4% at
210 550 K. The use of the TraPPE-UA force field yields the best prediction of
211 the experimental density of oX. The differences are of the order of two times

212 the statistical uncertainty for the considered temperature range, followed by
213 AUA, with three times the statistical error.

214 Significantly larger differences than in the liquid phase can be observed
215 in the vapor phase for the simulations and the experimental data. The calcu-
216 lated vapor densities are in agreement with the experiments at low temper-
217 atures (i.e. <450 K), and the differences arise at higher temperatures. The
218 vapor densities obtained with the TraPPE-UA and AUA force fields closely
219 follow the experimental data for mX. The highest deviations of the density
220 for every isomer are found with the OPLS force field. The largest differences
221 with the experimental data can be found for the oX vapor density at tem-
222 peratures over 450 K, where all force fields present deviations larger than the
223 statistical uncertainties from the experimental data. Such differences for oX
224 can be related to assumptions such as having fixed charges, a rigid molecule,
225 and transferable force field parameters for the three isomers. Assuming fixed
226 charges implies a fixed dipole/quadrupole moment. The aromatic π clouds re-
227 sult in a non-negligible quadrupole moment for the aromatic ring [41], which
228 is only considered by the AUA force field. The dipole polarization changes
229 with the temperature, specially for mX and oX [72], which is not considered
230 by any of the force fields.

231 The critical temperatures (T_c) and critical densities (ρ_c) are extrapolated
232 using the fitting procedure described by Dinpajoo et al. [73]. The obtained
233 critical points of mX, oX and pX for each force field are listed with experi-
234 mental data in Table 1. In general, the differences between the critical point
235 for each force field using the Wolf and Ewald methods are within the statisti-
236 cal error. This is related to the agreement found for the TraPPE-UA-EH and
237 AUA force fields shown in Fig. 4. However, the different densities obtained at
238 high temperature with the Wolf and the Ewald methods for the OPLS force
239 field have an impact on the determined critical point for xylene isomers. The
240 largest difference of the estimated critical temperature between the Wolf and
241 the Ewald methods is 14 K, for oX using the OPLS force field. The difference
242 of the critical point of the three isomers and the experimental data is smaller
243 than the statistical uncertainties for TraPPE-UA and AUA, as well as the
244 experimental critical point of pX is predicted by all the simulations within
245 the uncertainties.

246 3.2. Vapor-liquid Equilibria of binary mixtures

247 The VLE of the pX-oX binary mixture at 6.66 kPa is calculated with
248 *NPT*-Gibbs ensemble Monte Carlo simulations using the CFCMC method

249 [63]. The simulations are performed with each force field using the Ewald
250 and the Wolf methods. The phase compositions obtained with the TraPPE-
251 UA-EH, OPLS, and AUA force fields using the Wolf and Ewald methods
252 are shown in Fig. 5. It can be observed that the composition of the liquid
253 phase is not affected by the choice of force field or method for accounting the
254 electrostatic interactions. The statistical uncertainties are larger in the vapor
255 phase than in the liquid phase, and there is a reasonable agreement between
256 the calculated vapor phase compositions with both methods for electrostatic
257 interactions.

258 The phase diagrams of the pX-oX binary mixture at 6.66 kPa simulated
259 using the Ewald method with experimental data are shown in Fig. 6. Llopis
260 and Monton [21] reported discrete measurements of the phase composition
261 of the mixture. This data is shown as lines to facilitate comparison with the
262 simulations. The experimental uncertainties reported are 0.1 K for the tem-
263 perature and a standard deviation of 0.001 for reported mole fractions. Small
264 differences from ideality are reported [21] and a small difference between the
265 phase compositions is observed. The experimental data suggests that the
266 vapor does not have the same composition as the liquid. The component
267 with the lowest boiling temperature will have a higher molar fraction in the
268 vapor phase than that with the higher boiling temperature. The simulated
269 composition of the liquid phase is in excellent agreement with the experimen-
270 tal data and the differences are below the statistical uncertainties. Larger
271 differences can be observed for the composition of the vapor phase, where
272 simulations seem to predict an azeotrope behavior, as a phase composition
273 in the vapor equal to the liquid can be found at temperatures between 334
274 and 336 K. The mole fraction of pX in the vapor phase is higher than in the
275 liquid phase at temperatures higher than 335K, whereas an opposite behav-
276 ior is predicted by the simulations for temperatures lower than 334 K. This
277 suggests that the vapor phase composition of the component with the highest
278 mole fraction in the liquid phase is underestimated by the simulations. It is
279 important to note that the temperature range of these simulations is out of
280 the fitting range of the force fields, so the observed azeotropic behavior can
281 be an artifact of the force field.

282 The excess chemical potential of pX in the liquid phase of the pX/oX
283 mixture at 6.66 kPa, as a function of the liquid phase composition is shown
284 in Fig. 7. The reference state for the excess chemical potential is the ideal gas.
285 The excess chemical potential computed for each force field with the Wolf and
286 Ewald methods agree between the statistical uncertainties. A slight increase

287 of the excess chemical potential of pX in the liquid phase can be observed
288 as the mole fraction of pX increases in the mixture. However, this increase
289 is small and within the error bars. The excess chemical potential is directly
290 related to the activity coefficient of the component in the mixture [74, 75].
291 The activity coefficients for pX reported by the experimental work [21] do
292 not show dependence on the phase composition of the mixture, which is in
293 agreement with the excess chemical potential calculated in the simulations.

294 The phase diagrams of the pX-oX binary mixture at 81.3 kPa simulated
295 using the Ewald summation for all the force fields and experimental data
296 [23] are shown in Fig. 8. The reported experimental uncertainty for the tem-
297 peratures is 0.1 K. Small deviations from ideality are reported [23], and a
298 difference between the phase compositions smaller than in the binary mixture
299 at 6.66 kPa can be observed. Larger differences in the computed composition
300 of the liquid phase with the experiments than at 6.66 kPa are found. The
301 prediction of the liquid phase composition obtained using the TraPPE-UA
302 and TraPPE-UA-EH force fields show excellent agreement with experiments.
303 Small deviations from the experimental liquid phase composition are ob-
304 tained using the OPLS and AUA force fields when the phase composition
305 of oX is higher than for pX. The prediction of the composition of the va-
306 por phase obtained with the TraPPE-UA force field qualitatively predicts
307 the experimental composition of the vapor phase. However, the predictions
308 overestimate the mole fraction of pX in the vapor phase when the mole frac-
309 tion of oX is larger than for pX in the liquid phase. The simulations with the
310 rest of force fields yield an azeotrope as in the simulations at 6.66 kPa. This
311 suggests that the vapor phase composition of the component with the high-
312 est mole fraction in the liquid phase is underestimated by the simulations.
313 It can be concluded that for the tested force fields, the predictions of the
314 composition of the vapor phase are predominantly represented by the prop-
315 erties of the component with the largest mole fraction in the liquid phase.
316 The accuracy of the calculations are related to how well the densities can be
317 calculated for the pure components. The differences on the estimation of the
318 density of oX as a pure component play a significant role in the determination
319 of the VLE of binary mixtures of xylenes.

320 4. Conclusions

321 The VLE of xylenes as a single components and binary mixtures have
322 been calculated using the Wolf and Ewald methods. Comparable results

323 using the Wolf and the Ewald methods can be obtained for the prediction
324 of densities and the phase compositions of binary mixtures. With the Wolf
325 method, up to 50% less CPU time is used compared to the Ewald method, at
326 the cost of accuracy and additional parameter calibration. The performance
327 of the considered force fields to predict the VLE of xylene isomers as pure
328 component has been tested. The TraPPE-UA and AUA force fields provide
329 a reasonable estimate of the experimentally determined densities for pX and
330 mX. The largest differences with experimental data are observed in the cal-
331 culations of the vapor density of oX. The use of the TraPPE-UA force field
332 yields the best prediction of the experimental density of oX. Simulations of
333 pX/oX binary mixtures at 6.66 and 81.3 kPa are in excellent agreement with
334 the experimental data for the liquid phase composition. The predictions of
335 the composition of the vapor phase are dominated by the properties of the
336 component with the highest mole fraction in the liquid phase. The accuracy
337 of the phase composition predictions are related to the quality of the density
338 predictions of the pure component systems. The experimental vapor phase
339 composition is not well predicted by the simulations. This is related to the
340 deviations observed for the prediction of the vapor density of oX as a pure
341 component. For this reason, only a qualitative prediction of the vapor phase
342 composition was obtained using the TraPPE-UA force field for the pX-oX
343 binary mixture at 81.3 kPa. The simulations have shown the potential to
344 accurately predict the phase compositions of such binary mixture, but the
345 development of force fields that predict the VLE of each xylene isomer more
346 accurately -especially oX- is needed. The binary systems of xylenes are very
347 sensitive to the slight density differences in the vapor phase of each xylene
348 isomer and how well these are captured by the force fields.

349 **Acknowledgements**

350 This work was sponsored by NWO Exacte Wetenschappen (Physical Sci-
351 ences) for the use of supercomputer facilities, with financial support from the
352 Nederlandse Organisatie voor Wetenschappelijk Onderzoek (Netherlands Or-
353 ganization for Scientific Research, NWO). T.J.H.V. acknowledges NWO-CW
354 for a VICI grant. The authors also gratefully acknowledge financial support
355 from Shell Global Solutions B.V.

Table 1: Critical temperatures (T_c) and critical densities (ρ_c) of pure components extrapolated from VLE simulations using the fitting procedure described by Dinpajoooh et al. [73]. (E) and (W) denote the use of the Ewald and the Wolf methods, respectively. The numbers between round brackets denote the uncertainty in the last digit. Experimental data are from Refs. [76, 77, 78].

T_c /[K], ρ_c /[kg/m ³]	m-xylene		o-xylene		p-xylene	
	T_c	ρ_c	T_c	ρ_c	T_c	ρ_c
Experimental [76, 77, 78]	616.4(10)	283(4)	630.5(10)	287(4)	617.6(10)	281(4)
TraPPE-UA	620(7)	288(7)	629(7)	297(6)	617(4)	286(8)
TraPPE-UA-EH (E)	604(11)	279(7)	622(6)	278(5)	626(9)	279(6)
TraPPE-UA-EH (W)	610(9)	270(6)	623(5)	275(3)	620(7)	278(7)
OPLS (E)	605(9)	290(9)	626(8)	293(6)	609(8)	285(6)
OPLS (W)	609(9)	279(5)	612(9)	300(9)	611(9)	277(8)
AUA (E)	618(9)	284(6)	625(9)	293(6)	616(8)	290(6)
AUA (W)	618(9)	281(7)	627(8)	286(7)	616(14)	288(8)

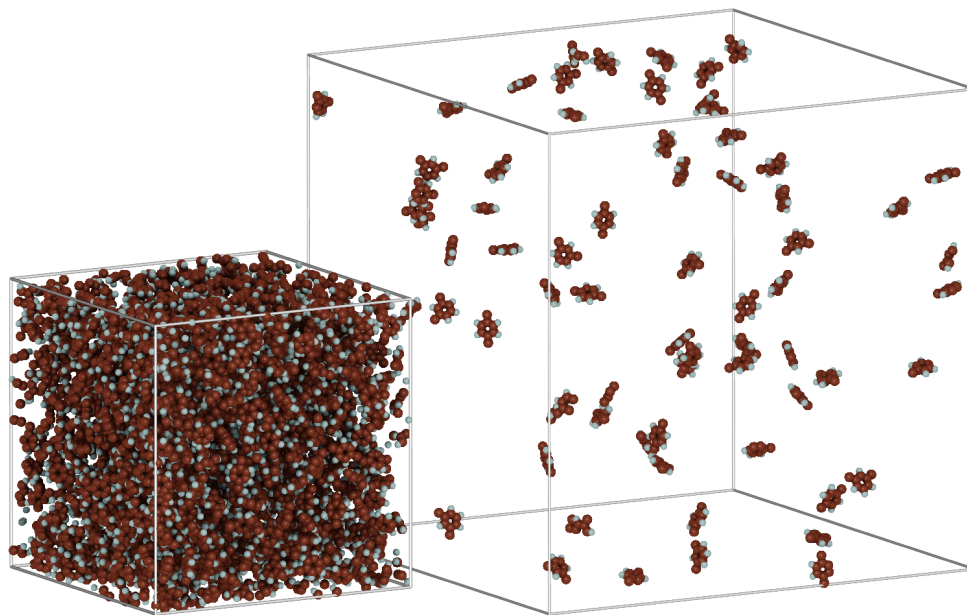


Figure 1: Schematic representation of the NPT -Gibbs Ensemble MC simulation of the pX - mX binary mixture. The two boxes represent the liquid (left) and vapor (right) phases. Figure rendered with the iRASP visualization software [79].

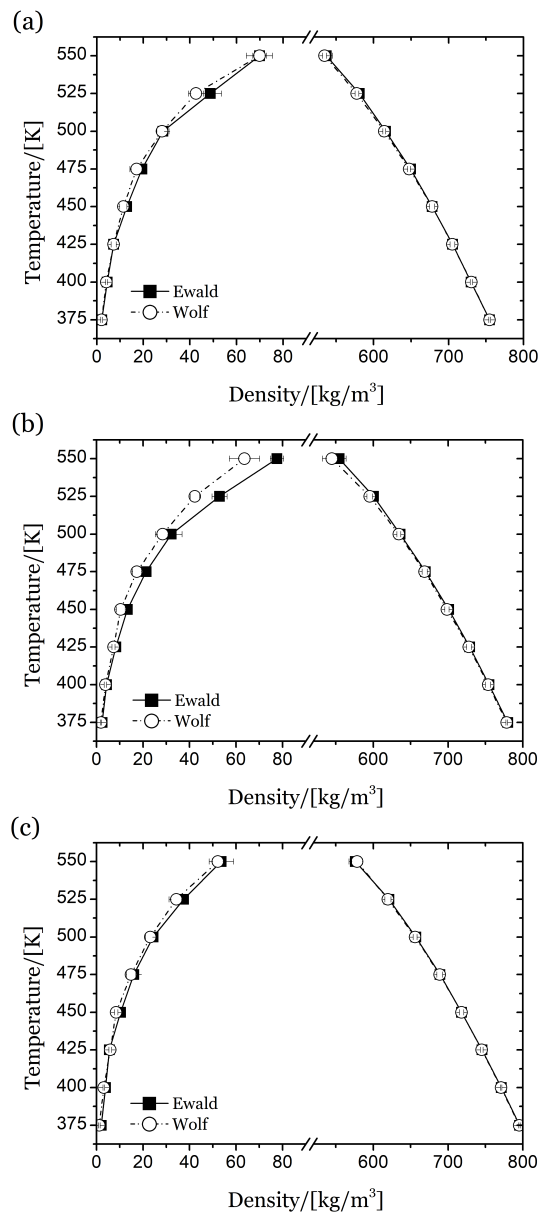


Figure 2: VLE of m-xylene for different force fields using the Ewald (closed symbol) and the Wolf (open symbol) methods. (a) TraPPE-UA-EH [41, 34], (b) OPLS [42], (c) AUA [37]. Tabulated data with the uncertainties are listed in the Supporting Information.

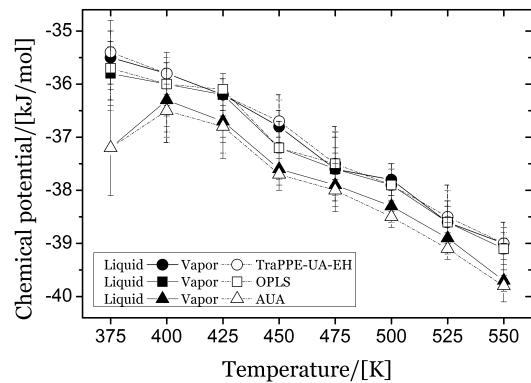


Figure 3: Chemical potential of m-xylene at VLE coexistence as a function of temperature using the Wolf method for each force field. Closed and open symbols represent the liquid and vapor boxes, respectively. Tabulated data with the uncertainties are listed in the Supporting Information.

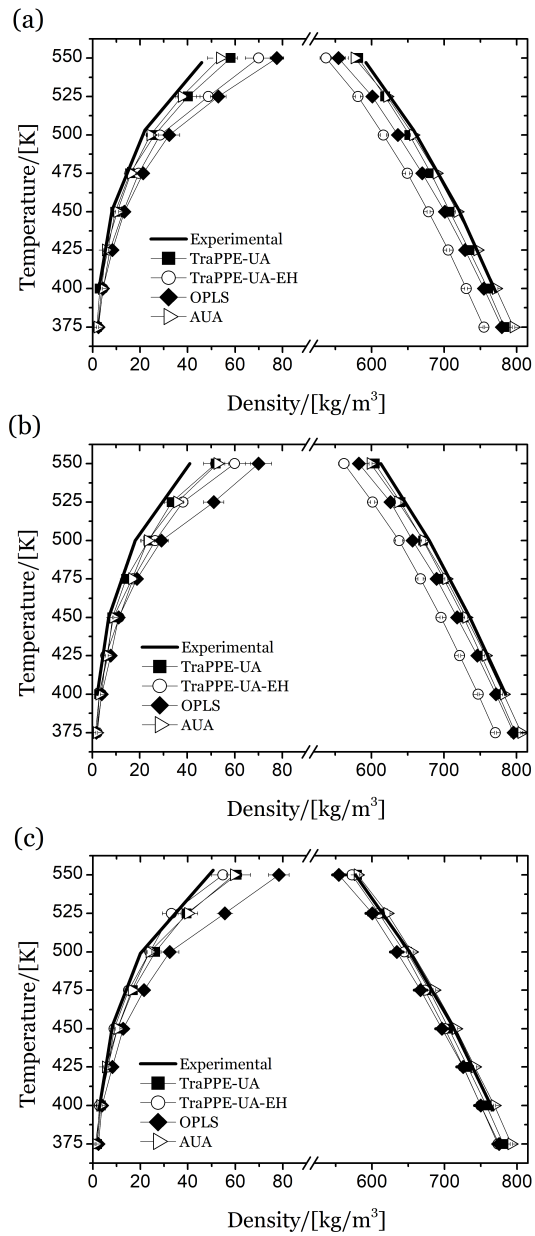


Figure 4: Vapor-liquid equilibria of (a) m-xylene, (b) o-xylene, and (c) p-xylene for each force field using the Ewald summation method. Experimental data from Ref. [17] is also included. Tabulated data with the uncertainties are listed in the Supporting Information.

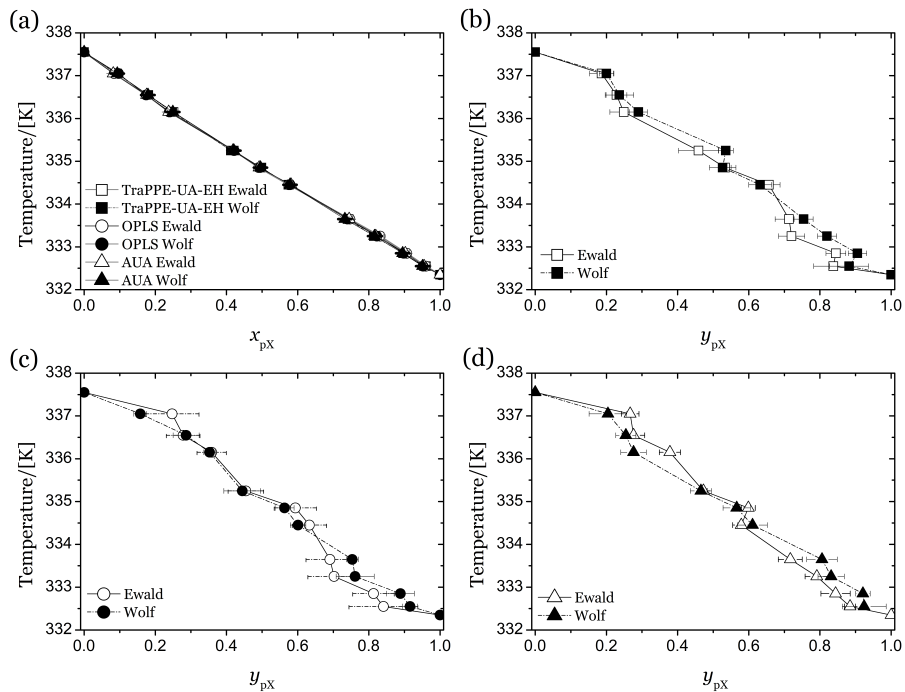


Figure 5: Phase composition diagrams of the p-xylene/o-xylene binary mixture at 6.66 kPa using the Wolf and Ewald methods. (a) Liquid phase composition for TraPPE-UA-EH [41, 34], OPLS [42] and AUA [37] force fields. Vapor phase composition for (b) TraPPE-UA-EH [41, 34], (c) OPLS [42], and (d) AUA [37]. x_{pX} is the mole fraction of pX in the liquid phase. y_{pX} is the mole fraction of pX in the vapor phase. Closed and open symbols represent the values using the Wolf and the Ewald method, respectively. Tabulated data with the uncertainties are listed in the Supporting Information.

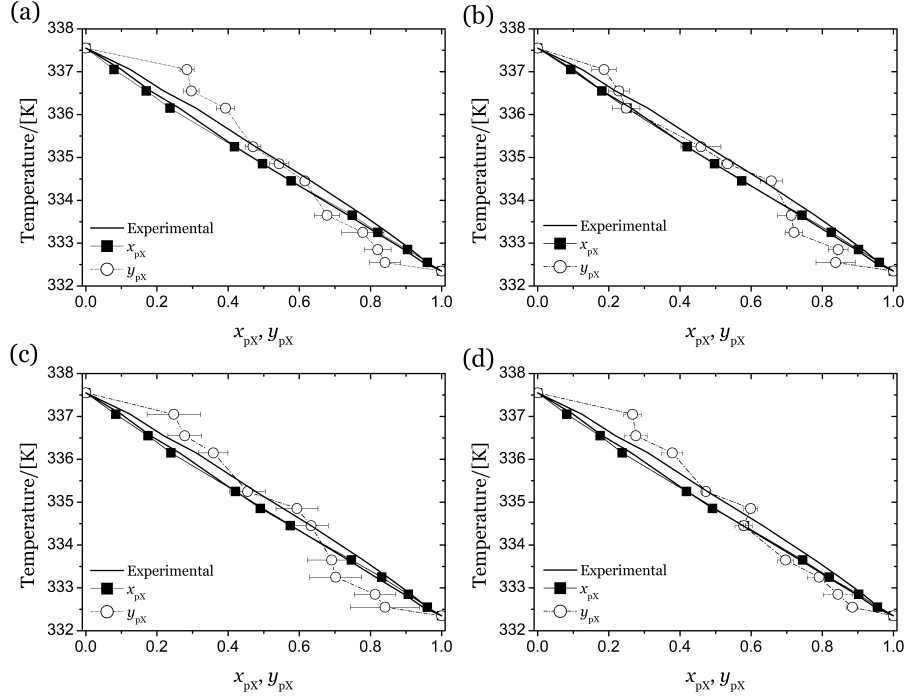


Figure 6: Phase diagram of the p-xylene/o-xylene binary mixture at 6.66 kPa for (a) TraPPE-UA [41], (b) TraPPE-UA-EH [41, 34], (c) OPLS [42], and (d) AUA [37], calculated using the Ewald method. Experimental data are from Llopis and Monton [21]. x_{pX} (closed symbols) is the mole fraction of pX in the liquid phase. y_{pX} (open symbols) is the mole fraction of pX in the vapor phase. Tabulated data with the uncertainties are listed in the Supporting Information.

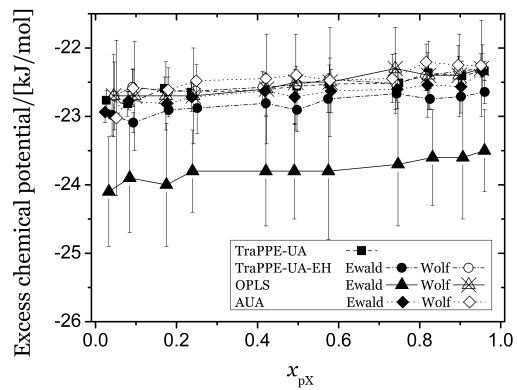


Figure 7: Excess chemical potential (μ^e_{pX}) of p-xylene in the liquid phase of the pX/oX binary mixture at 6.66 kPa, as a function of the liquid phase composition for all force fields. Closed and open symbols denote the use of the Ewald and the Wolf methods, respectively. Tabulated data with the uncertainties are listed in the Supporting Information.

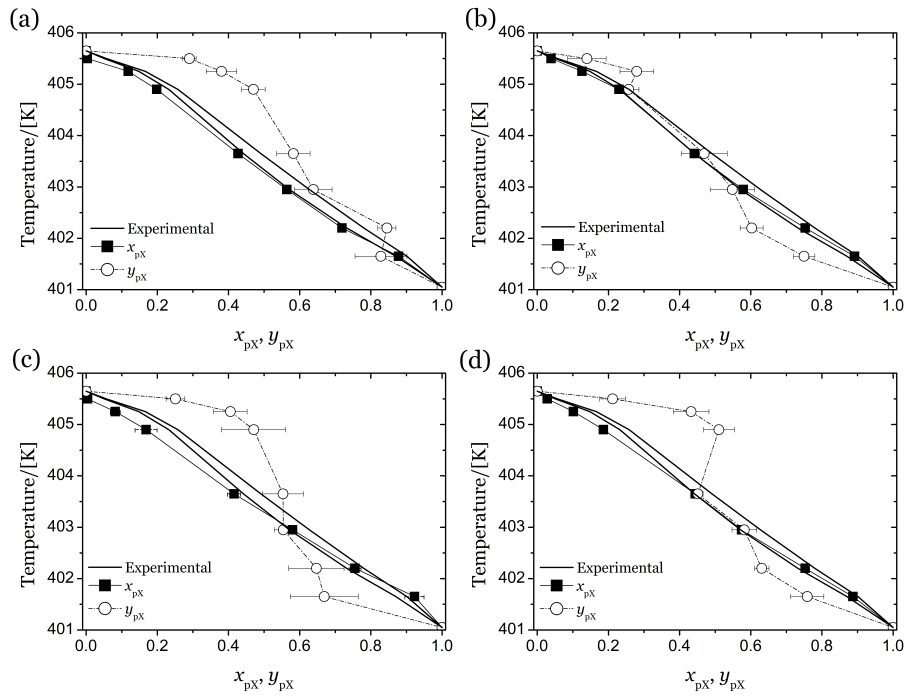


Figure 8: Phase diagram of the p-xylene/o-xylene binary mixture at 81.3 kPa for (a) TraPPE-UA [41], (b) TraPPE-UA-EH [41, 34], (c) OPLS [42], and (d) AUA [37], calculated using the Ewald method. Experimental data are from Parvez et al [23]. x_{pX} (closed symbols) is the mole fraction of pX in the liquid phase. y_{pX} (open symbols) is the mole fraction of pX in the vapor phase. Tabulated data with the uncertainties are listed in the Supporting Information.

356 **5. References**

- 357 [1] Y. Yang, P. Bai, X. Guo, Separation of Xylene Isomers: A Review
358 of Recent Advances in Materials, Industrial & Engineering Chemistry
359 Research 56 (2017) 14725–14753.
- 360 [2] J. Das, Y. Bhat, A. Halgeri, Aromatization of C₄-C₆ hydrocarbons to
361 benzene, toluene and para xylene over pore size controlled ZnO-HZSM-5
362 zeolite, in: T. S. R. P. Rao, G. M. Dhar (Eds.), Recent Advances In
363 Basic and Applied Aspects of Industrial Catalysis, volume 113 of *Studies*
364 *in Surface Science and Catalysis*, Elsevier, 1998, pp. 447 – 453.
- 365 [3] C. J. Egan, R. V. Luthy, Separation of Xylenes, Industrial & Engineering
366 Chemistry 47 (1955) 250–253.
- 367 [4] R. A. F. Tomás, J. C. M. Bordado, J. F. P. Gomes, p-Xylene Oxidation
368 to Terephthalic Acid: A Literature Review Oriented toward Process
369 Optimization and Development, Chemical Reviews 113 (2013) 7421–
370 7469.
- 371 [5] M. Minceva, A. Rodrigues, Adsorption of Xylenes on Faujasite-Type
372 Zeolite: Equilibrium and Kinetics in Batch Adsorber, Chemical Engi-
373 neering Research and Design 82 (2004) 667 – 681.
- 374 [6] W. J. Cannella, Xylenes and ethylbenzene, in: Kirk-Othmer Encyclo-
375 pedia of Chemical Technology, American Cancer Society, 2007.
- 376 [7] D. Stoye, W. Freitag, Paints, Coatings and Solvents, Wiley-Blackwell,
377 2nd edition, 2007.
- 378 [8] Z.-Y. Gu, X.-P. Yan, Metal-Organic Framework MIL-101 for High-
379 Resolution Gas-Chromatographic Separation of Xylene Isomers and
380 Ethylbenzene, Angewandte Chemie International Edition 49 (2010)
381 1477–1480.
- 382 [9] M. T. Ashraf, R. Chebbi, N. A. Darwish, Process of p-Xylene Production
383 by Highly Selective Methylation of Toluene, Industrial & Engineering
384 Chemistry Research 52 (2013) 13730–13737.
- 385 [10] Y. Ma, F. Zhang, S. Yang, R. P. Lively, Evidence for entropic diffu-
386 sion selection of xylene isomers in carbon molecular sieve membranes,
387 Journal of Membrane Science 564 (2018) 404 – 414.

- 388 [11] Y. Zhou, J. Wu, E. W. Lemmon, Thermodynamic Properties of o-
389 Xylene, m-Xylene, p-Xylene, and Ethylbenzene, *Journal of Physical*
390 *and Chemical Reference Data* 41 (2012) 023103.
- 391 [12] D. S. Sholl, R. P. Lively, Seven chemical separations to change the world,
392 *Nature* 532 (2016) 435–437.
- 393 [13] A. E. Rodrigues, C. Pereira, M. Minceva, L. S. Pais, A. M. Ribeiro,
394 A. Ribeiro, M. Silva, N. Graa, J. C. Santos, Chapter 5 - The Parex
395 Process for the Separation of p-Xylene, in: A. E. Rodrigues, C. Pereira,
396 M. Minceva, L. S. Pais, A. M. Ribeiro, A. Ribeiro, M. Silva, N. Graa,
397 J. C. Santos (Eds.), *Simulated Moving Bed Technology*, Butterworth-
398 Heinemann, Oxford, 2015, pp. 117 – 144.
- 399 [14] S. R. Dey, K. M. Ng, Fractional crystallization: Design alternatives and
400 tradeoffs, *AIChE Journal* 41 (1995) 2427–2438.
- 401 [15] H. Mohameed, B. A. Jdayil, K. Takrouri, Separation of para-xylene
402 from xylene mixture via crystallization, *Chemical Engineering and Pro-*
403 *cessing: Process Intensification* 46 (2007) 25 – 36.
- 404 [16] M. O. Daramola, A. J. Burger, M. Pera-Titus, A. Giroir-Fendler, S. Mi-
405 achon, J.-A. Dalmon, L. Lorenzen, Separation and isomerization of
406 xylenes using zeolite membranes: a short overview, *Asia-Pacific Journal*
407 *of Chemical Engineering* 5 (2010) 815–837.
- 408 [17] B. D. Smith, R. Srivastava, *Thermodynamic data for pure compound:*
409 *Part A, Hydrocarbons and Ketones*, Elsevier, Amsterdam, 1986.
- 410 [18] W. Rodrigues, S. Mattedi, J. C. N. Abreu, Experimental vapor-liquid
411 equilibria data for binary mixtures of xylene isomers, *Brazilian Journal*
412 *of Chemical Engineering* 22 (2005) 453 – 462.
- 413 [19] M. Kato, T. Sato, M. Hirata, Vapor-liquid equilibrium relationship of
414 para-xylene meta-xylene system at atmospheric pressure, *Journal of*
415 *Chemical Engineering of Japan* 4 (1971) 305–308.
- 416 [20] U. Onken, W. Arlt, *Recommended test mixtures for distillation columns*,
417 *IChemE*, 2nd edition, 1990.

- 418 [21] F. J. Llopis, J. B. Monton, Isobaric vapor-liquid equilibria of p-xylene
419 + o-xylene and m-xylene + o-xylene systems at 6.66 and 26.66 kPa,
420 Journal of Chemical & Engineering Data 39 (1994) 53–55.
- 421 [22] F. J. Llopis, J. B. Monton, Isobaric Vapor-Liquid Equilibria for Bi-
422 nary and Ternary Systems Composed of 1,4-Dimethylbenzene, 1,3-
423 Dimethylbenzene, and 1,2-Dimethylbenzene at 6.66 and 26.66 kPa,
424 Journal of Chemical & Engineering Data 39 (1994) 643–646.
- 425 [23] M. Parvez, G. Singh, S. Tyagi, S. Kumar, S. Khan, Experimental de-
426 termination of vapour-liquid equilibrium data for the binary mixtures
427 P-Xylene and O-Xylene at 81.3 kPa, Journal of Scientific and Technical
428 Advancements 1 (2015) 263–265.
- 429 [24] I. Wichterle, J. Linek, Z. Wagner, J.-C. Fontaine, K. Sosnkowska-
430 Kehiaian, H. Kehiaian, Vapor-Liquid Equilibrium of the Mixture C_8H_{10}
431 + C_8H_{10} (LB3761, EVLM 1211), in: H. Kehiaian (Ed.), Binary Liquid
432 Systems of Nonelectrolytes. Part 2, Springer Berlin Heidelberg, Berlin,
433 Heidelberg, 2008, pp. 1221–1222.
- 434 [25] D. Frenkel, B. Smit, Understanding Molecular Simulation, Academic
435 Press, 2nd edition, 2002.
- 436 [26] A. Z. Panagiotopoulos, M. R. Stapleton, The Gibbs method for
437 molecular-based computer simulations of phase equilibria, Fluid Phase
438 Equilibria 53 (1989) 133 – 141. Proceedings of the Fifth International
439 Conference.
- 440 [27] M. Ramdin, S. H. Jamali, T. M. Becker, T. J. H. Vlugt, Gibbs ensem-
441 ble Monte Carlo simulations of multicomponent natural gas mixtures,
442 Molecular Simulation 44 (2018) 377–383.
- 443 [28] A. Panagiotopoulos, N. Quirke, M. Stapleton, D. Tildesley, Phase equi-
444 libria by simulation in the Gibbs ensemble, Molecular Physics 63 (1988)
445 527–545.
- 446 [29] A. D. Cortés Morales, I. G. Economou, C. J. Peters, J. I. Siepmann,
447 Influence of simulation protocols on the efficiency of Gibbs ensemble
448 Monte Carlo simulations, Molecular Simulation 39 (2013) 1135–1142.

- 449 [30] M. Ramdin, T. M. Becker, S. H. Jamali, M. Wang, T. J. H. Vlugt,
450 Computing equation of state parameters of gases from Monte Carlo
451 simulations, *Fluid Phase Equilibria* 428 (2016) 174 – 181.
- 452 [31] P. Ungerer, C. Nieto-Draghi, B. Rousseau, G. Ahunbay, V. Lachet,
453 Molecular simulation of the thermophysical properties of fluids: From
454 understanding toward quantitative predictions, *Journal of Molecular*
455 *Liquids* 134 (2007) 71 – 89.
- 456 [32] P. Ungerer, B. Tavitian, A. Boutin, *Applications of Molecular Simu-*
457 *lation in the Oil and Gas Industry - Monte-Carlo Methods*, Editions
458 Technip, 1st edition, 2005.
- 459 [33] A. Torres-Knoop, N. C. Burtch, A. Poursaeidesfahani, S. P. Balaji,
460 R. Kools, F. X. Smit, K. S. Walton, T. J. Vlugt, D. Dubbeldam,
461 Optimization of Particle Transfers in the Gibbs Ensemble for Systems
462 with Strong and Directional Interactions Using CBMC, CFCMC, and
463 CB/CFCMC, *Journal of Physical Chemistry C* 120 (2016) 9148–9159.
- 464 [34] N. Rai, J. I. Siepmann, Transferable Potentials for Phase Equilibria.
465 9. Explicit Hydrogen Description of Benzene and Five-Membered and
466 Six-Membered Heterocyclic Aromatic Compounds, *Journal of Physical*
467 *Chemistry B* 111 (2007) 10790–10799.
- 468 [35] N. Rai, J. I. Siepmann, Transferable Potentials for Phase Equilibria. 10.
469 Explicit-Hydrogen Description of Substituted Benzenes and Polycyclic
470 Aromatic Compounds, *Journal of Physical Chemistry B* 117 (2013)
471 273–288.
- 472 [36] P. Bonnaud, C. Nieto-Draghi, P. Ungerer, Anisotropic United Atom
473 Model Including the Electrostatic Interactions of Benzene, *The Journal*
474 *of Physical Chemistry B* 111 (2007) 3730–3741.
- 475 [37] C. Nieto-Draghi, P. Bonnaud, P. Ungerer, Anisotropic United Atom
476 Model Including the Electrostatic Interactions of Methylbenzenes. I.
477 Thermodynamic and Structural Properties, *Journal of Physical Chem-*
478 *istry C* 111 (2007) 15686–15699.
- 479 [38] I. Cacelli, G. Cinacchi, G. Prampolini, A. Tani, Computer Simulation
480 of Solid and Liquid Benzene with an Atomistic Interaction Potential

- 481 Derived from ab Initio Calculations, *Journal of the American Chemical*
482 *Society* 126 (2004) 14278–14286.
- 483 [39] P. E. M. Lopes, G. Lamoureux, B. Roux, A. D. MacKerell, Polarizable
484 Empirical Force Field for Aromatic Compounds Based on the Classical
485 Drude Oscillator, *Journal of Physical Chemistry B* 111 (2007) 2873–
486 2885.
- 487 [40] H. Sun, COMPASS: An ab Initio Force-Field Optimized for Condensed-
488 Phase Applications - Overview with Details on Alkane and Benzene
489 Compounds, *Journal of Physical Chemistry B* 102 (1998) 7338–7364.
- 490 [41] C. D. Wick, M. G. Martin, J. I. Siepmann, Transferable Potentials for
491 Phase Equilibria. 4. United-Atom Description of Linear and Branched
492 Alkenes and Alkylbenzenes, *Journal of Physical Chemistry B* 104 (2000)
493 8008–8016.
- 494 [42] W. L. Jorgensen, E. R. Laird, T. B. Nguyen, J. Tirado-Rives, Monte
495 Carlo simulations of pure liquid substituted benzenes with OPLS poten-
496 tial functions, *Journal of Computational Chemistry* 14 (1993) 206–215.
- 497 [43] A. K. Rappe, C. J. Casewit, K. S. Colwell, W. A. Goddard, W. M.
498 Skiff, UFF, a full periodic table force field for molecular mechanics and
499 molecular dynamics simulations, *Journal of the American Chemical*
500 *Society* 114 (1992) 10024–10035.
- 501 [44] K. Chenoweth, A. C. T. van Duin, W. A. Goddard, ReaxFF Reac-
502 tive Force Field for Molecular Dynamics Simulations of Hydrocarbon
503 Oxidation, *Journal of Physical Chemistry A* 112 (2008) 1040–1053.
- 504 [45] P. P. Ewald, Die Berechnung optischer und elektrostatischer Gitterpo-
505 tentiale, *Annalen der Physik* 369 (1921) 253–287.
- 506 [46] B. A. Wells, A. L. Chaffee, Ewald Summation for Molecular Simulations,
507 *Journal of Chemical Theory and Computation* 11 (2015) 3684–3695.
- 508 [47] J. W. Eastwood, R. W. Hockney, D. N. Lawrence, P3M3DP The three-
509 dimensional periodic particle-particle/particle-mesh program, *Com-
510 puter Physics Communications* 19 (1980) 215 – 261.

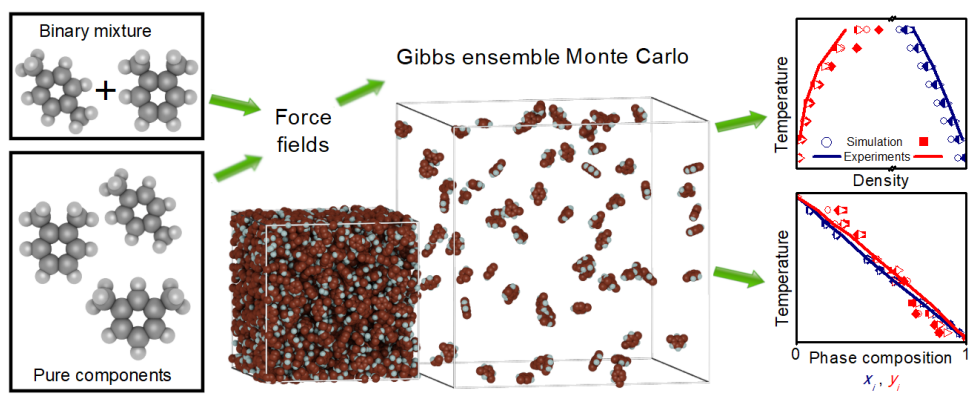
- 511 [48] L. Onsager, Electric Moments of Molecules in Liquids, *Journal of the*
512 *American Chemical Society* 58 (1936) 1486–1493.
- 513 [49] L. Greengard, V. Rokhlin, A fast algorithm for particle simulations,
514 *Journal of Computational Physics* 73 (1987) 325 – 348.
- 515 [50] D. Wolf, P. Koblinski, S. R. Phillpot, J. Eggebrecht, Exact method for
516 the simulation of Coulombic systems by spherically truncated, pairwise
517 r^{-1} summation, *Journal of Chemical Physics* 110 (1999) 8254–8282.
- 518 [51] A. Cisneros, M. Karttunen, P. Ren, C. Sagui, Classical Electrostatics
519 for Biomolecular Simulations, *Chemical Reviews* 114 (2014) 779–814.
- 520 [52] G. S. Fanourgakis, An Extension of Wolf’s Method for the Treatment
521 of Electrostatic Interactions: Application to Liquid Water and Aqueous
522 Solutions, *Journal of Physical Chemistry B* 119 (2015) 1974–1985.
- 523 [53] P. Demontis, S. Spanu, G. B. Suffritti, Application of the Wolf method
524 for the evaluation of Coulombic interactions to complex condensed mat-
525 ter systems: Aluminosilicates and water, *Journal of Chemical Physics*
526 114 (2001) 7980–7988.
- 527 [54] C. Avendaño, A. Gil-Villegas, Monte Carlo simulations of primitive
528 models for ionic systems using the Wolf method, *Molecular Physics* 104
529 (2006) 1475–1486.
- 530 [55] P. X. Viveros-Méndez, A. Gil-Villegas, Computer simulation of sedi-
531 mentation of ionic systems using the Wolf method, *Journal of Chemical*
532 *Physics* 136 (2012) 154507.
- 533 [56] D. Zahn, B. Schilling, S. M. Kast, Enhancement of the Wolf Damped
534 Coulomb Potential: Static, Dynamic, and Dielectric Properties of Liquid
535 Water from Molecular Simulation, *Journal of Physical Chemistry B* 106
536 (2002) 10725–10732.
- 537 [57] C. J. Fennell, J. D. Gezelter, Is the Ewald summation still necessary?
538 Pairwise alternatives to the accepted standard for long-range electro-
539 statics, *Journal of Chemical Physics* 124 (2006) 234104.
- 540 [58] J. Kolafa, F. Močka, I. Nezbeda, Handling Electrostatic Interactions in
541 Molecular Simulations: A systematic study, *Collection of Czechoslovak*
542 *Chemical Communications* 73 (2008) 481–506.

- 543 [59] A. Rahbari, R. Hens, S. H. Jamali, M. Ramdin, D. Dubbeldam, T. J. H.
544 Vlugt, Effect of truncating electrostatic interactions on predicting ther-
545 modynamic properties of water-methanol systems, *Molecular Simulation*
546 (2018).
- 547 [60] R. Hens, T. J. H. Vlugt, Molecular Simulation of Vapor-liquid Equi-
548 libria Using the Wolf Method for Electrostatic Interactions, *Journal of*
549 *Chemical & Engineering Data* 63 (2018) 1096–1102.
- 550 [61] C. Waibel, J. Gross, Modification of the Wolf Method and Evaluation for
551 Molecular Simulation of Vapor Liquid Equilibria, *Journal of Chemical*
552 *Theory and Computation* 14 (2018) 2198–2206.
- 553 [62] M. P. Allen, D. Tildesley, *Computer Simulation of liquids*, Oxford Uni-
554 versity Press, 2nd edition, 2017.
- 555 [63] A. Poursaeidesfahani, A. Torres-Knoop, D. Dubbeldam, T. J. H. Vlugt,
556 Direct Free Energy Calculation in the Continuous Fractional Component
557 Gibbs Ensemble, *Journal of Chemical Theory and Computation* 12
558 (2016) 1481–1490.
- 559 [64] A. Poursaeidesfahani, A. Rahbari, A. Torres-Knoop, D. Dubbeldam,
560 T. J. H. Vlugt, Computation of thermodynamic properties in the con-
561 tinuous fractional component Monte Carlo Gibbs ensemble, *Molecular*
562 *Simulation* 43 (2017) 189–195.
- 563 [65] A. Rahbari, R. Hens, I. K. Nikolaidis, A. Poursaeidesfahani, M. Ramdin,
564 I. G. Economou, O. A. Moulτος, D. Dubbeldam, T. J. H. Vlugt, Compu-
565 tation of partial molar properties using continuous fractional component
566 Monte Carlo, *Molecular Physics* 116 (2018) 3331–3344.
- 567 [66] D. Dubbeldam, S. Calero, D. E. Ellis, R. Q. Snurr, RASPA: molecular
568 simulation software for adsorption and diffusion in flexible nanoporous
569 materials, *Molecular Simulation* 42 (2016) 81–101.
- 570 [67] D. Dubbeldam, A. Torres-Knoop, K. S. Walton, On the inner workings
571 of Monte Carlo codes, *Molecular Simulation* 39 (2013) 1253–1292.
- 572 [68] F. Wang, D. P. Landau, Efficient, Multiple-Range Random Walk Algo-
573 rithm to Calculate the Density of States, *Physical Review Letters* 86
574 (2001) 2050–2053.

- 575 [69] W. L. Jorgensen, D. S. Maxwell, J. Tirado-Rives, Development and
576 Testing of the OPLS All-Atom Force Field on Conformational Energetics
577 and Properties of Organic Liquids, *Journal of the American Chemical*
578 *Society* 118 (1996) 11225–11236.
- 579 [70] J. M. Castillo, T. J. H. Vlugt, S. Calero, Molecular Simulation Study on
580 the Separation of Xylene Isomers in MIL-47 Metal-Organic Frameworks,
581 *Journal of Physical Chemistry C* 113 (2009) 20869–20874.
- 582 [71] C. Nieto-Draghi, P. Bonnaud, P. Ungerer, Anisotropic United Atom
583 Model Including the Electrostatic Interactions of Methylbenzenes. II.
584 Transport Properties, *Journal of Physical Chemistry C* 111 (2007)
585 15942–15951.
- 586 [72] H. Kanai, V. Inouye, L. Yazawa, R. Goo, H. Wakatsuki, Importance of
587 Debye and Keesom interactions in separating m-xylene and p-xylene in
588 GC-MS analysis utilizing PEG stationary phase, *Journal of Chromato-*
589 *graphic Science* 43 (2005) 57–62.
- 590 [73] M. Dinpajoo, P. Bai, D. A. Allan, J. I. Siepmann, Accurate and precise
591 determination of critical properties from Gibbs ensemble Monte Carlo
592 simulations, *Journal of Chemical Physics* 143 (2015) 114113.
- 593 [74] S. Hempel, J. Fischer, D. Paschek, G. Sadowski, Activity Coefficients
594 of Complex Molecules by Molecular Simulation and Gibbs-Duhem Inte-
595 gration, *Soft Materials* 10 (2012) 26–41.
- 596 [75] S. P. Balaji, S. K. Schnell, E. S. McGarrity, T. J. H. Vlugt, A direct
597 method for calculating thermodynamic factors for liquid mixtures using
598 the Permuted Widom test particle insertion method, *Molecular Physics*
599 111 (2013) 287–296.
- 600 [76] R. D. Chirico, S. E. Knipmeyer, A. Nguyen, J. W. Reynolds, W. V.
601 Steele, Thermodynamic Equilibria in Xylene Isomerization. 2. The Ther-
602 modynamic Properties of m-Xylene, *Journal of Chemical & Engineering*
603 *Data* 42 (1997) 475–487.
- 604 [77] R. D. Chirico, S. E. Knipmeyer, A. Nguyen, A. B. Cowell, J. W.
605 Reynolds, W. V. Steele, Thermodynamic Equilibria in Xylene Iso-
606 merization. 3. The Thermodynamic Properties of o-Xylene, *Journal*
607 *of Chemical & Engineering Data* 42 (1997) 758–771.

- 608 [78] R. D. Chirico, S. E. Knipmeyer, A. Nguyen, W. V. Steele, Thermo-
609 dynamic Equilibria in Xylene Isomerization. 1. The Thermodynamic
610 Properties of p-Xylene, *Journal of Chemical & Engineering Data* 42
611 (1997) 248–261.
- 612 [79] D. Dubbeldam, S. Calero, T. J. H. Vlugt, iRASP: GPU-accelerated
613 visualization software for materials scientists, *Molecular Simulation* 44
614 (2018) 653–676.

Graphical Abstract



Supporting Information

Molecular Simulation of the Vapor-Liquid Equilibria of Xylene mixtures: Force Field performance, and Wolf vs. Ewald for Electrostatic Interactions

Sebastián Caro-Ortiz^a, Remco Hens^a, Erik Zuidema^b, Marcello Rigutto^b, David Dubbeldam^c, and Thijs J. H. Vlugt^{a*}

^a*Engineering Thermodynamics, Process & Energy Department, Faculty of Mechanical, Maritime and Materials Engineering, Delft University of Technology Leeghwaterstraat 39, 2628 CB Delft, The Netherlands.*

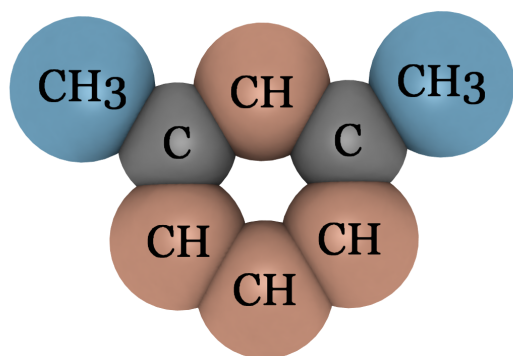
^b*Shell Global Solutions International, PO Box 38000, 1030 BN, Amsterdam, The Netherlands.*

^c*Van 't Hoff Institute of Molecular Sciences, University of Amsterdam, Science Park 904, 1098 XH Amsterdam, The Netherlands.*

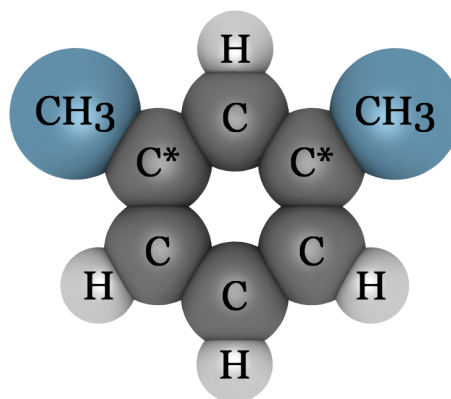
E-mail: t.j.h.vlugt@tudelft.nl

Table S1: Force field parameters for xylene isomers. All molecules are considered as rigid. For the atom positions, the reader is referred to the original publications of the force fields¹⁻⁶.

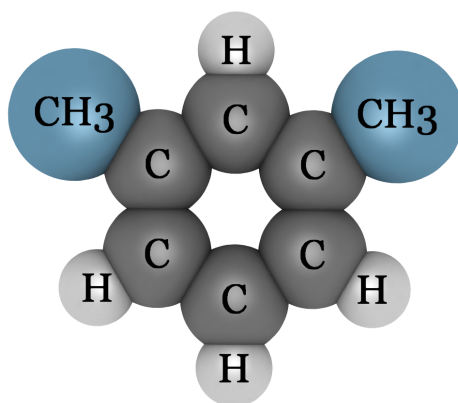
Force field	Atom	ϵ/k_B / [K]	σ / [Å]	q / [e]
TraPPE-UA ¹	C	21.00	3.880	0
	CH	50.50	3.695	0
	CH ₃	98.00	3.750	0
TraPPEE-UA-EH ^{1,2}	C	30.70	3.600	-0.095
	C*	21.00	3.880	0
	H	25.50	2.360	0.095
	CH ₃	98.00	3.750	0
OPLS ^{3,4}	C	35.24	3.550	-0.115
	H	15.03	2.420	0.115
	CH ₃	85.51	3.800	0.115
AUA ^{5,6}	C	35.43	3.361	0
	CH	75.60	3.361	0
	CH ₃	120.15	3.607	0
	Center site (+)	0	0	8.130
	π -site (-)	0	0	-4.065



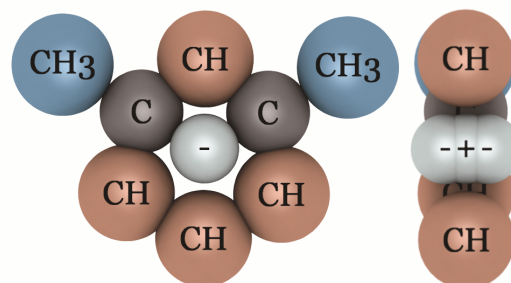
(a) TraPPE-UA



(b) TraPPE-UA-EH



(c) OPLS



(d) AUA

Figure 1: Schematic representation of m-xylene for the (a) TraPPE-UA¹, (b) TraPPE-UA-EH^{1,2}, (c) OPLS^{3,4}, and (d) AUA^{5,6} force fields. Atom labels use the notation of Table S1. Figure rendered with the iRASPA visualization software⁷.

Table S2: VLE simulation input for m-xylene, o-xylene and p-xylene. T is the temperature, N the number of molecules, L the initial length of one side of the (cubic) simulation box. The subscripts l and v indicate the liquid and vapor boxes, respectively.

T /[K]	N_l	N_v	L_l /[Å]	L_v /[Å]
375	965	35	60	142
400	933	67	60	142
425	899	101	60	130
450	863	137	60	126
475	830	170	60	114
500	797	203	60	112
525	760	240	60	112
550	745	255	60	105

Table S3: VLE simulation results for liquid densities (ρ_l) and vapor densities (ρ_v) of m-xylene, o-xylene, and p-xylene for different temperatures (T) obtained with the TraPPE-UA force field. The numbers between round brackets denote the uncertainties in the last digit.

T /[K]	m-xylene		o-xylene		p-xylene	
	ρ_l /[kg/m ³]	ρ_v /[kg/m ³]	ρ_l /[kg/m ³]	ρ_v /[kg/m ³]	ρ_l /[kg/m ³]	ρ_v /[kg/m ³]
375	783(1)	1.8(3)	799(1)	1.4(2)	781(2)	1.8(5)
400	760(1)	3.1(1)	775(2)	2.9(6)	758(2)	3.4(5)
425	734(1)	6.3(11)	752(2)	6.5(7)	732(2)	6.2(7)
450	708(3)	9.5(8)	727(3)	8.4(12)	706(2)	10.4(7)
475	682(2)	16(2)	699(4)	14(2)	679(1)	17(4)
500	652(4)	26(4)	671(2)	24(3)	648(4)	26(2)
525	618(3)	40(5)	640(1)	34(3)	615(4)	39(2)
550	581(3)	58(3)	605(3)	52(5)	579(5)	61(6)

Table S4: VLE simulation results for liquid densities (ρ_l) and vapor densities (ρ_v) of m-xylene, o-xylene, and p-xylene for different temperatures (T) obtained with the TraPPE-UA-EH force field using the Ewald and the Wolf methods. The numbers between round brackets denote the uncertainties in the last digit.

Ewald	m-xylene		o-xylene		p-xylene		
	T /[K]	ρ_l /[kg/m ³]	ρ_v /[kg/m ³]	ρ_l /[kg/m ³]	ρ_v /[kg/m ³]	ρ_l /[kg/m ³]	ρ_v /[kg/m ³]
	375	755(1)	2.2(4)	771(2)	2.0(2)	774(2)	1.7(4)
	400	730(2)	4.5(3)	747(2)	3.8(5)	750(2)	2.8(5)
	425	706(2)	7.2(9)	722(2)	6(2)	726(2)	6.5(7)
	450	678(2)	13(2)	696(2)	11(1)	700(2)	9(1)
	475	649(3)	19(1)	668(4)	17(2)	673(1)	15(2)
	500	616(5)	28(3)	638(5)	27(3)	644(4)	24(3)
	525	581(3)	49(5)	601(3)	38(3)	609(3)	33(4)
	550	537(8)	70(6)	562(8)	60(7)	572(6)	55(5)

Wolf	m-xylene		o-xylene		p-xylene		
	T /[K]	ρ_l /[kg/m ³]	ρ_v /[kg/m ³]	ρ_l /[kg/m ³]	ρ_v /[kg/m ³]	ρ_l /[kg/m ³]	ρ_v /[kg/m ³]
	375	755(2)	2.1(4)	771(2)	1.8(1)	773(2)	1.5(3)
	400	731(2)	4.1(3)	747(2)	3.6(4)	750(1)	3.2(9)
	425	705(4)	7(2)	722(4)	6.3(5)	727(3)	5(2)
	450	679(4)	11(2)	695(2)	10(1)	700(1)	9(1)
	475	647(2)	17(3)	667(2)	167(1)	673(2)	15(1)
	500	614(2)	28(2)	635(3)	25(3)	643(4)	22(2)
	525	578(3)	43(3)	603(4)	40(2)	610(3)	35(5)
	550	535(3)	70(3)	558(3)	56(6)	570(4)	49(8)

Table S5: VLE simulation results for liquid densities (ρ_l) and vapor densities (ρ_v) of m-xylene, o-xylene, and p-xylene for different temperatures (T) obtained with the OPLS force field using the Ewald and the Wolf methods. The numbers between round brackets denote the uncertainties in the last digit.

Ewald	m-xylene		o-xylene		p-xylene	
	T /[K]	ρ_l /[kg/m ³]	ρ_v /[kg/m ³]	ρ_l /[kg/m ³]	ρ_v /[kg/m ³]	ρ_l /[kg/m ³]
375	780(2)	2.4(4)	796(3)	1.7(3)	775(3)	2.3(5)
400	755(3)	4.3(7)	772(2)	4(1)	750(1)	3.9(3)
425	729(2)	8.3(8)	746(3)	8(1)	726(2)	8(1)
450	701(2)	13(1)	718(1)	11(2)	696(2)	13(2)
475	670(3)	21(2)	670(1)	19(2)	667(3)	22(2)
500	636(2)	32(5)	657(2)	29(3)	634(4)	32(4)
525	601(5)	53(3)	627(5)	51(5)	600(5)	56(3)
550	555(9)	78(3)	583(5)	70(6)	554(5)	78(5)

Wolf	m-xylene		o-xylene		p-xylene	
	T /[K]	ρ_l /[kg/m ³]	ρ_v /[kg/m ³]	ρ_l /[kg/m ³]	ρ_v /[kg/m ³]	ρ_l /[kg/m ³]
375	778(2)	1.9(2)	796(3)	1.5(3)	775(2)	1.8(4)
400	753(4)	3.8(5)	772(1)	3.5(1)	750(2)	3.3(4)
425	728(3)	7.3(7)	745(3)	6.8(2)	724(3)	6.3(7)
450	698(3)	10(2)	717(4)	10(2)	697(2)	12(2)
475	669(4)	17(2)	689(3)	18(3)	665(3)	17(2)
500	634(3)	28(3)	656(1)	25(1)	631(5)	28(2)
525	595(4)	42(2)	615(5)	36(4)	590(7)	39(6)
550	545(13)	64(7)	571(5)	52(4)	541(4)	62(2)

Table S6: VLE simulation results for liquid densities (ρ_l) and vapor densities (ρ_v) of m-xylene, o-xylene, and p-xylene for different temperatures (T) obtained with the AUA force field using the Ewald and the Wolf methods. The numbers between round brackets denote the uncertainties in the last digit.

Ewald	m-xylene		o-xylene		p-xylene	
	ρ_l /[kg/m ³]	ρ_v /[kg/m ³]	ρ_l /[kg/m ³]	ρ_v /[kg/m ³]	ρ_l /[kg/m ³]	ρ_v /[kg/m ³]
375	796(2)	2.1(4)	807(2)	1.9(4)	792(2)	1.1(3)
400	771(3)	3.9(4)	782(2)	2.9(5)	769(2)	3.1(8)
425	746(1)	6(1)	757(2)	6.1(6)	742(2)	5.4(9)
450	718(3)	10(1)	731(2)	8.7(3)	716(3)	10(1)
475	689(5)	16(2)	703(2)	17(2)	686(2)	16(3)
500	657(4)	24(2)	672(3)	23(3)	655(2)	24(1)
525	621(5)	38(2)	637(4)	36(3)	621(4)	40(4)
550	576(9)	54(6)	599(2)	53(3)	580(2)	60(3)

Wolf	m-xylene		o-xylene		p-xylene	
	ρ_l /[kg/m ³]	ρ_v /[kg/m ³]	ρ_l /[kg/m ³]	ρ_v /[kg/m ³]	ρ_l /[kg/m ³]	ρ_v /[kg/m ³]
375	795(1)	1.2(4)	806(2)	1.2(4)	793(1)	1.5(2)
400	771(1)	3.2(4)	782(2)	2.7(5)	768(1)	2.7(2)
425	745(2)	5.9(6)	758(2)	4.4(3)	743(2)	5(1)
450	718(3)	8.4(7)	730(2)	9(2)	715(3)	9(2)
475	689(4)	15(2)	703(1)	15(2)	686(1)	16(2)
500	656(3)	23(2)	668(3)	18(3)	655(2)	23(2)
525	620(4)	34(3)	636(3)	33(3)	620(6)	37(3)
550	579(7)	52(3)	594(7)	47(7)	578(5)	57(1)

Table S7: Chemical potentials (μ) of m-xylene, o-xylene, and p-xylene for different temperatures (T) obtained with the TraPPE-UA force field. The subscripts l and v indicate the liquid and vapor boxes, respectively. The numbers between round brackets denote the uncertainties in the last digit.

T /[K]	m-xylene		o-xylene		p-xylene	
	μ_l /[kJ/mol]	μ_v /[kJ/mol]	μ_l /[kJ/mol]	μ_v /[kJ/mol]	μ_l /[kJ/mol]	μ_v /[kJ/mol]
375	-36.0(5)	-35.9(4)	-36.9(5)	-36.8(3)	-35.9(7)	-35.9(6)
400	-36.8(3)	-36.7(2)	-36.8(5)	-36.8(6)	-36.4(3)	-36.3(4)
425	-36.6(7)	-36.5(6)	-36.5(4)	-36.4(4)	-36.7(3)	-36.7(4)
450	-37.3(5)	-37.2(5)	-37.7(6)	-37.8(6)	-37.2(3)	-37.1(2)
475	-37.8(4)	-37.8(5)	-38.0(3)	-38.1(3)	-37.7(4)	-37.6(5)
500	-38.0(4)	-38.1(5)	-38.3(5)	-38.3(3)	-38.1(2)	-38.1(1)
525	-38.7(4)	-38.7(5)	-39.0(2)	-39.1(2)	-38.6(3)	-38.7(1)
550	-39.2(2)	-39.4(2)	-39.7(2)	-39.7(4)	-39.3(4)	-39.3(3)

Table S8: Chemical potentials (μ) of m-xylene, o-xylene, and p-xylene for different temperatures (T) obtained with the TraPPE-UA-EH force field using the Wolf and Ewald methods. The subscripts l and v indicate the liquid and vapor boxes, respectively. The numbers between round brackets denote the uncertainties in the last digit.

Ewald	m-xylene		o-xylene		p-xylene	
T /[K]	μ_l /[kJ/mol]	μ_v /[kJ/mol]	μ_l /[kJ/mol]	μ_v /[kJ/mol]	μ_l /[kJ/mol]	μ_v /[kJ/mol]
375	-35.6(4)	-35.5(5)	-35.9(2)	-35.9(2)	-36.3(7)	-36.3(6)
400	-35.8(2)	-35.7(2)	-36.2(4)	-36.1(3)	-37.1(4)	-37.0(5)
425	-36.4(2)	-36.4(3)	-37.2(8)	-37.2(7)	-36.6(4)	-36.7(3)
450	-36.6(4)	-36.6(3)	-37.0(4)	-37.1(3)	-37.7(4)	-37.8(5)
475	-37.2(3)	-37.3(3)	-37.7(2)	-37.7(2)	-38.1(3)	-38.1(4)
500	-38.1(1)	-38.0(2)	-38.3(2)	-38.3(2)	-38.5(2)	-38.6(4)
525	-38.3(4)	-38.3(3)	-39.0(3)	-39.0(2)	-39.3(2)	-39.3(3)
550	-38.9(3)	-39.0(3)	-39.5(4)	-39.5(3)	-39.8(4)	-39.8(5)

Wolf	m-xylene		o-xylene		p-xylene	
T /[K]	μ_l /[kJ/mol]	μ_v /[kJ/mol]	μ_l /[kJ/mol]	μ_v /[kJ/mol]	μ_l /[kJ/mol]	μ_v /[kJ/mol]
375	-35.5(5)	-35.4(6)	-36.0(3)	-35.9(3)	-36.5(5)	-36.4(5)
400	-35.8(1)	-35.8(2)	-36.2(4)	-36.1(4)	-36.5(7)	-36.5(6)
425	-36.2(3)	-36.2(4)	-36.7(3)	-36.6(4)	-37.2(9)	-37.2(7)
450	-36.8(3)	-36.7(4)	-37.3(4)	-37.2(5)	-37.6(6)	-37.6(5)
475	-37.6(6)	-37.5(6)	-37.6(2)	-37.7(2)	-38.0(3)	-38.0(1)
500	-37.8(3)	-37.9(3)	-38.3(3)	-38.3(2)	-38.6(4)	-38.6(1)
525	-38.6(3)	-38.5(3)	-38.8(2)	-38.7(1)	-39.2(1)	-39.2(3)
550	-39.0(1)	-39.0(2)	-39.6(3)	-39.6(1)	-39.8(4)	-39.9(4)

Table S9: Chemical potentials (μ) of m-xylene, o-xylene, and p-xylene for different temperatures (T) obtained with the OPLS force field using the Wolf and Ewald methods. The subscripts l and v indicate the liquid and vapor boxes, respectively. The numbers between round brackets denote the uncertainties in the last digit.

Ewald	m-xylene		o-xylene		p-xylene	
T /[K]	μ_l /[kJ/mol]	μ_v /[kJ/mol]	μ_l /[kJ/mol]	μ_v /[kJ/mol]	μ_l /[kJ/mol]	μ_v /[kJ/mol]
375	-35.8(5)	-35.8(6)	-36.9(4)	-36.9(4)	-35.8(7)	-35.8(6)
400	-36.4(7)	-36.3(7)	-36.7(9)	-36.7(8)	-36.6(4)	-36.6(5)
425	-36.4(2)	-36.4(2)	-36.6(3)	-36.5(4)	-36.5(4)	-36.4(5)
450	-36.9(2)	-36.9(2)	-37.5(4)	-37.5(3)	-37.0(7)	-37.1(5)
475	-37.3(5)	-37.3(4)	-37.7(3)	-37.6(3)	-37.3(2)	-37.3(4)
500	-37.9(2)	-37.8(3)	-38.2(3)	-38.2(5)	-37.9(3)	-37.9(4)
525	-38.4(2)	-38.4(2)	-38.4(2)	-38.5(1)	-38.3(3)	-38.3(2)
550	-39.0(1)	-39.2(2)	-39.3(2)	-39.4(3)	-39.1(2)	-39.0(2)

Wolf	m-xylene		o-xylene		p-xylene	
T /[K]	μ_l /[kJ/mol]	μ_v /[kJ/mol]	μ_l /[kJ/mol]	μ_v /[kJ/mol]	μ_l /[kJ/mol]	μ_v /[kJ/mol]
375	-35.8(3)	-35.7(4)	-36.3(6)	-36.3(5)	-36.1(5)	-36.0(5)
400	-36.0(4)	-36.0(4)	-36.2(3)	-36.2(4)	-36.5(5)	-36.4(4)
425	-36.2(4)	-36.1(3)	-36.4(2)	-36.4(1)	-36.6(6)	-36.5(6)
450	-37.2(4)	-37.2(5)	-37.3(5)	-37.3(3)	-36.6(3)	-36.6(4)
475	-37.6(3)	-37.5(3)	-37.4(5)	-37.4(5)	-37.6(3)	-37.6(4)
500	-37.9(3)	-37.9(3)	-38.2(5)	-38.2(4)	-37.8(1)	-37.8(3)
525	-38.6(4)	-38.6(3)	-39.0(4)	-38.9(4)	-38.7(4)	-38.7(3)
550	-39.1(4)	-39.1(2)	-39.6(4)	-39.7(4)	-39.2(2)	-39.3(2)

Table S10: Chemical potentials (μ) of m-xylene, o-xylene, and p-xylene for different temperatures (T) obtained with the AUA force field using the Wolf and Ewald methods. The subscripts l and v indicate the liquid and vapor boxes, respectively. The numbers between round brackets denote the uncertainties in the last digit.

Ewald	m-xylene		o-xylene		p-xylene	
T /[K]	μ_l /[kJ/mol]	μ_v /[kJ/mol]	μ_l /[kJ/mol]	μ_v /[kJ/mol]	μ_l /[kJ/mol]	μ_v /[kJ/mol]
375	-35.5(5)	-35.4(6)	-35.8(5)	-35.7(6)	-37.5(7)	-37.3(6)
400	-35.9(5)	-35.9(5)	-36.8(5)	-36.8(5)	-36.6(7)	-36.5(8)
425	-37.0(4)	-36.9(5)	-36.6(3)	-36.6(4)	-37.2(4)	-37.1(4)
450	-37.1(3)	-37.1(3)	-37.6(1)	-37.6(2)	-37.1(3)	-37.1(2)
475	-37.5(3)	-37.6(3)	-37.4(5)	-37.4(4)	-37.6(4)	-37.6(4)
500	-38.2(2)	-38.2(2)	-38.3(5)	-38.3(4)	-38.2(2)	-38.2(2)
525	-38.7(2)	-38.7(1)	-38.8(3)	-38.8(1)	-38.5(5)	-38.5(2)
550	-39.5(3)	-39.5(2)	-39.5(2)	-39.5(1)	-39.2(3)	-39.2(2)

Wolf	m-xylene		o-xylene		p-xylene	
T /[K]	μ_l /[kJ/mol]	μ_v /[kJ/mol]	μ_l /[kJ/mol]	μ_v /[kJ/mol]	μ_l /[kJ/mol]	μ_v /[kJ/mol]
375	-37.2(9)	-37.2(9)	-37.1(6)	-37.1(7)	-36.3(5)	-36.4(5)
400	-36.3(3)	-36.5(3)	-37.1(7)	-37.2(7)	-37.0(3)	-37.1(3)
425	-36.7(3)	-36.8(3)	-37.6(3)	-37.8(1)	-37.3(6)	-37.4(4)
450	-37.6(3)	-37.7(3)	-37.5(5)	-37.7(5)	-37.5(5)	-37.7(4)
475	-37.9(4)	-38.0(4)	-37.9(4)	-38.1(4)	-37.7(4)	-37.9(3)
500	-38.3(2)	-38.5(2)	-39.0(5)	-39.1(4)	-38.5(2)	-38.7(4)
525	-38.9(1)	-39.1(2)	-39.0(3)	-39.1(4)	-38.9(3)	-39.0(4)
550	-39.7(2)	-39.8(3)	-39.9(4)	-40.0(4)	-39.3(4)	-39.5(5)

Table S11: VLE phase composition for the p-xylene/o-xylene binary mixture at 6.66 kPa for each force field and experimental data⁸. (E) and (W) denote the use of the Ewald and the Wolf methods, respectively. x_{pX} is the mole fraction of pX in the liquid phase. y_{pX} is the mole fraction of pX in the vapor phase. The numbers between round brackets denote the uncertainties in the last digit.

$T/[\text{K}]$	Experimental ⁸		TraPPE-UA		TraPPE-UA-EH (E)		TraPPE-UA-EH (W)	
	x_{pX}	y_{pX}	x_{pX}	y_{pX}	x_{pX}	y_{pX}	x_{pX}	y_{pX}
332.55	0.948(1)	0.959(1)	0.960(5)	0.841(44)	0.961(6)	0.838(55)	0.955(5)	0.882(54)
332.85	0.895(1)	0.915(1)	0.904(4)	0.821(37)	0.902(3)	0.845(28)	0.896(2)	0.906(26)
333.25	0.815(1)	0.849(1)	0.821(6)	0.778(59)	0.825(2)	0.720(37)	0.814(2)	0.819(25)
333.65	0.738(1)	0.780(1)	0.749(4)	0.678(35)	0.743(3)	0.713(39)	0.740(2)	0.754(27)
334.45	0.577(1)	0.633(1)	0.577(2)	0.616(13)	0.574(3)	0.657(31)	0.576(3)	0.632(32)
334.85	0.497(1)	0.555(1)	0.497(3)	0.544(27)	0.497(2)	0.533(17)	0.499(4)	0.527(37)
335.25	0.420(1)	0.477(1)	0.418(3)	0.470(22)	0.421(6)	0.459(56)	0.413(2)	0.535(21)
336.15	0.263(1)	0.310(1)	0.237(4)	0.393(25)	0.251(4)	0.249(39)	0.247(2)	0.290(25)
336.55	0.182(1)	0.219(1)	0.170(3)	0.296(22)	0.181(3)	0.228(29)	0.180(4)	0.236(40)
337.05	0.100(1)	0.125(1)	0.079(3)	0.284(20)	0.093(4)	0.186(34)	0.091(2)	0.200(20)

$T/[\text{K}]$	OPLS (E)		OPLS (W)		AUA(E)		AUA (W)	
	x_{pX}	y_{pX}	x_{pX}	y_{pX}	x_{pX}	y_{pX}	x_{pX}	y_{pX}
332.55	0.960(11)	0.841(97)	0.952(2)	0.916(22)	0.955(2)	0.884(16)	0.951(5)	0.924(62)
332.85	0.907(7)	0.813(58)	0.898(3)	0.889(39)	0.902(4)	0.844(41)	0.895(2)	0.921(20)
333.25	0.832(11)	0.702(73)	0.822(5)	0.761(53)	0.820(3)	0.791(33)	0.816(3)	0.831(37)
333.65	0.747(8)	0.691(67)	0.740(2)	0.753(17)	0.745(2)	0.717(34)	0.732(2)	0.806(43)
334.45	0.575(5)	0.633(48)	0.579(2)	0.601(22)	0.581(3)	0.579(24)	0.579(4)	0.610(42)
334.85	0.491(7)	0.593(59)	0.494(3)	0.563(27)	0.492(2)	0.599(20)	0.496(3)	0.566(38)
335.25	0.421(6)	0.454(50)	0.422(5)	0.444(52)	0.418(1)	0.473(10)	0.421(2)	0.465(29)
336.15	0.239(5)	0.358(41)	0.241(2)	0.353(17)	0.237(3)	0.378(30)	0.249(3)	0.276(36)
336.55	0.175(6)	0.278(47)	0.174(3)	0.287(37)	0.176(4)	0.276(32)	0.179(3)	0.255(28)
337.05	0.084(10)	0.247(75)	0.097(2)	0.158(18)	0.082(4)	0.267(25)	0.093(5)	0.204(53)

Table S12: Excess chemical potential (μ_{pX}^e) of p-xylene in the liquid phase of the p-xylene/o-xylene binary mixture at 6.66 kPa for different temperatures (T) and different force fields. (E) and (W) denote the use of the Ewald and the Wolf methods, respectively. The numbers between round brackets denote the uncertainties in the last digit.

T /[K]	TraPPE-UA	TraPPE-UA-EH	
	μ_{pX}^e /[kJ/mol]	μ_{pX}^e /[kJ/mol] (E)	μ_{pX}^e /[kJ/mol] (W)
332.55	-22.3(1)	-22.6(2)	-22.3(3)
332.85	-22.4(2)	-22.7(2)	-22.3(2)
333.25	-22.4(1)	-22.7(1)	-22.4(2)
333.65	-22.5(2)	-22.7(1)	-22.5(4)
334.45	-22.5(3)	-22.7(2)	-22.5(1)
334.85	-22.6(2)	-22.9(3)	-22.5(1)
335.25	-22.6(2)	-22.8(2)	-22.6(2)
336.15	-22.6(1)	-22.9(4)	-22.6(1)
336.55	-22.6(2)	-22.9(1)	-22.6(3)
337.05	-22.8(2)	-23.1(1)	-22.6(3)
337.25	-22.8(1)	-23.0(3)	-22.7(5)

T /[K]	OPLS		AUA	
	μ_{pX}^e /[kJ/mol] (E)	μ_{pX}^e /[kJ/mol] (W)	μ_{pX}^e /[kJ/mol] (E)	μ_{pX}^e /[kJ/mol] (W)
332.55	-23.5(6)	-22.3(7)	-22.3(3)	-22.3(2)
332.85	-23.6(9)	-22.4(6)	-22.6(2)	-22.3(3)
333.25	-23.6(7)	-22.4(5)	-22.5(5)	-22.2(3)
333.65	-23.7(9)	-22.3(6)	-22.6(3)	-22.4(4)
334.45	-23.8(10)	-22.5(8)	-22.6(3)	-22.5(3)
334.85	-23.8(7)	-22.5(7)	-22.7(4)	-22.4(1)
335.25	-23.8(8)	-22.6(8)	-22.6(2)	-22.4(1)
336.15	-23.8(6)	-22.7(7)	-22.7(2)	-22.5(2)
336.55	-24.0(9)	-22.7(5)	-22.8(1)	-22.6(2)
337.05	-23.9(8)	-22.7(8)	-22.8(1)	-22.6(3)
337.25	-24.1(8)	-22.7(6)	-22.9(2)	-23.0(1)

Table S13: VLE phase composition for the p-xylene/o-xylene binary mixture at 81.3 kPa for each force field using the Ewald method, and experimental data⁹. x_{pX} is the mole fraction of pX in the liquid phase. y_{pX} is the mole fraction of pX in the vapor phase. The numbers between round brackets denote the uncertainties in the last digit.

$T/[\text{K}]$	Experimental ⁹		TraPPE-UA		TraPPE-UA-EH	
	x_{pX}	y_{pX}	x_{pX}	y_{pX}	x_{pX}	y_{pX}
401.65	0.870	0.901	0.878(10)	0.828(73)	0.891(5)	0.750(30)
402.20	0.732	0.780	0.719(5)	0.845(25)	0.753(5)	0.602(32)
402.95	0.571	0.627	0.564(9)	0.638(53)	0.579(9)	0.548(63)
403.65	0.442	0.491	0.427(7)	0.582(47)	0.441(9)	0.469(65)
404.90	0.232	0.258	0.198(4)	0.470(33)	0.230(5)	0.257(28)
405.25	0.148	0.166	0.118(5)	0.380(43)	0.126(11)	0.280(47)
405.50	0.051	0.057	0.003(1)	0.290(19)	0.039(8)	0.139(54)

$T/[\text{K}]$	OPLS		AUA	
	x_{pX}	y_{pX}	x_{pX}	y_{pX}
401.65	0.923(27)	0.669(95)	0.887(6)	0.759(47)
402.20	0.755(17)	0.647(78)	0.753(4)	0.631(20)
402.95	0.580(6)	0.554(26)	0.574(4)	0.582(35)
403.65	0.416(18)	0.553(57)	0.444(3)	0.451(15)
404.90	0.169(31)	0.471(90)	0.186(7)	0.510(43)
405.25	0.082(14)	0.405(47)	0.102(9)	0.432(50)
405.50	0.004(7)	0.251(26)	0.028(7)	0.212(36)

References

- (1) Wick, C. D.; Martin, M. G.; Siepmann, J. I. Transferable Potentials for Phase Equilibria. 4. United-Atom Description of Linear and Branched Alkenes and Alkylbenzenes. *Journal of Physical Chemistry B* **2000**, *104*, 8008–8016.
- (2) Rai, N.; Siepmann, J. I. Transferable Potentials for Phase Equilibria. 9. Explicit Hydrogen Description of Benzene and Five-Membered and Six-Membered Heterocyclic Aromatic Compounds. *Journal of Physical Chemistry B* **2007**, *111*, 10790–10799.
- (3) Jorgensen, W. L.; Laird, E. R.; Nguyen, T. B.; Tirado-Rives, J. Monte Carlo simulations of pure liquid substituted benzenes with OPLS potential functions. *Journal of Computational Chemistry* **1993**, *14*, 206–215.
- (4) Jorgensen, W. L.; Maxwell, D. S.; Tirado-Rives, J. Development and Testing of the OPLS All-Atom Force Field on Conformational Energetics and Properties of Organic Liquids. *Journal of the American Chemical Society* **1996**, *118*, 11225–11236.
- (5) Nieto-Draghi, C.; Bonnaud, P.; Ungerer, P. Anisotropic United Atom Model Including the Electrostatic Interactions of Methylbenzenes. I. Thermodynamic and Structural Properties. *Journal of Physical Chemistry C* **2007**, *111*, 15686–15699.
- (6) Nieto-Draghi, C.; Bonnaud, P.; Ungerer, P. Anisotropic United Atom Model Including the Electrostatic Interactions of Methylbenzenes. II. Transport Properties. *Journal of Physical Chemistry C* **2007**, *111*, 15942–15951.
- (7) Dubbeldam, D.; Calero, S.; Vlugt, T. J. H. iRASPA: GPU-accelerated visualization software for materials scientists. *Molecular Simulation* **2018**, *44*, 653–676.
- (8) Llopis, F. J.; Monton, J. B. Isobaric vapor-liquid equilibria of p-xylene + o-xylene and m-xylene + o-xylene systems at 6.66 and 26.66 kPa. *Journal of Chemical & Engineering Data* **1994**, *39*, 53–55.

- (9) Parvez, M.; Singh, G.; Tyagi, S.; Kumar, S.; Khan, S. Experimental determination of vapour-liquid equilibrium data for the binary mixtures P-Xylene and O-Xylene at 81.3 kPa. *Journal of Scientific and Technical Advancements* **2015**, *1*, 263–265.